ACS APPLIED MATERIALS & INTERFACES

www.acsami.org

Research Article

Elastic Microstructures: Combining Biochemical, Mechanical, and Topographical Cues for the Effective Activation and Proliferation of Cytotoxic T Cells

Ashish Pandey, Muhammed Iraqi, Esti Toledo, Abed Al-Kader Yassin, Eytan Podvalni, Shagufta Naaz, Jatin Jawhir Pandit, Carlos Ureña Martin, Guillaume Le Saux, Angel Porgador, and Mark Schvartzman*

Cite This: *ACS Appl. Mater. Interfaces* 2023, 15, 31103−31113

Read Online

ACCESS | Metrics & More | Article Recommendations | Supporting Information

ABSTRACT: The ex vivo activation and proliferation of cytotoxic T cells are critical steps in adoptive immunotherapy. Today, T cells are activated by stimulation with antibody-coated magnetic beads, traditionally used for cell separation. Yet, efficient and controlled activation and proliferation of T cells require new antibody-bearing materials, which, in particular, deliver mechanical and topographic cues sensed by T cells. Here, we demonstrate a new approach for the activation and proliferation of human cytotoxic T cells using an elastic microbrush coated with activating and costimulatory antibodies. We found that the microbrush topography affects the protrusion of the cell membrane and the elastic response to the forces applied by cells and can be optimized to yield the strongest activation of T cells. In particular, T cells stimulated by a microbrush showed a three-fold increase in degranulation and release of cytokines over T cells stimulated with state-of-the-art magnetic beads. Furthermore, the microbrush induced a T-cell proliferation of T cells that was more prolonged and yielded much higher cell doubling than that done by the state-of-the-art methods. Our study provides an essential insight into the physical mechanism of T-cell activation and proliferation and opens the floodgates for the design of novel stimulatory materials for T-cell-based immunotherapy.

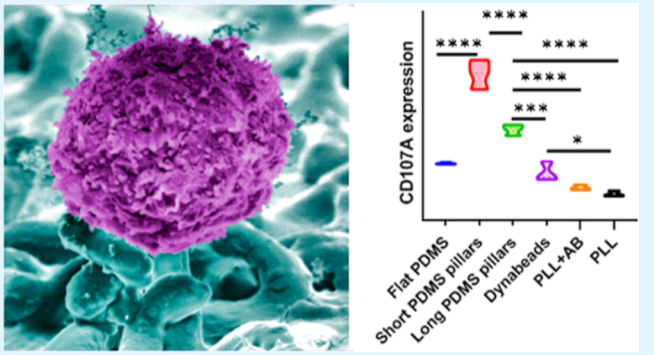

KEYWORDS: *T cells, activation, proliferation, PDMS microbrushes, immunotherapy*

INTRODUCTION

Adoptive immunotherapy is a new, rapidly developing family of approaches to treat cancer with a patient's own lymphocytes. It includes chimeric antigen receptor (CAR) T-cell immunotherapy, which is based on T cells transfected with engineered receptors consisting of (i) an antibody-based extracellular domain specific to a cancer marker and (ii) an intracellular domain that generates activating and costimulatory signaling. The engineered T cells are then transfused back to the patient's body and attack the tumor.[1] Today, several CAR T-cell immunotherapies are approved by FDA for the treatment of B-cell acute lymphoblastic leukemia, B-cell non-Hodgkin's lymphoma, and multiple myeloma. Another emerging approach of immunotherapy is based on tumor-infiltrating lymphocytes (TILs), which are isolated from the tumor stroma, assayed for neoantigen-specific recognition, and expanded before re-introduction to the patient.[2,3] The advantage of TIL-based therapy over other adoptive T-cell therapies stems from its great tumor-homing ability, low off-target toxicity, and it showed promising clinical responses in metastatic melanoma,[4] advanced cervical cancer,[5] epithelial lung cancer,[6] colorectal cancer,[7] and breast cancer.[8] Additional adoptive immunotherapies employ T cells with engineered T-cell receptors and natural killer (NK) cells. With more than 1000 ongoing or recruiting clinical trials, according to www.clinicaltrials.gov, these methods altogether promise to revolutionize cancer treatment in the coming years.

Despite encouraging developments in T-cell-based immunotherapy, it still faces several key challenges. One of them is related to the ex vivo activation and expansion steps in the process of immunotherapeutic T-cell production, which are critical for obtaining a therapeutically sufficient amount of T cells and their efficient transfection with CARs. Today, T cells are commonly activated prior their proliferation using magnetic beads coated with antibodies that engage activating

Received: February 10, 2023
Accepted: June 6, 2023
Published: June 22, 2023

https://doi.org/10.1021/acsami.3c01871
ACS Appl. Mater. Interfaces 2023, 15, 31103−31113

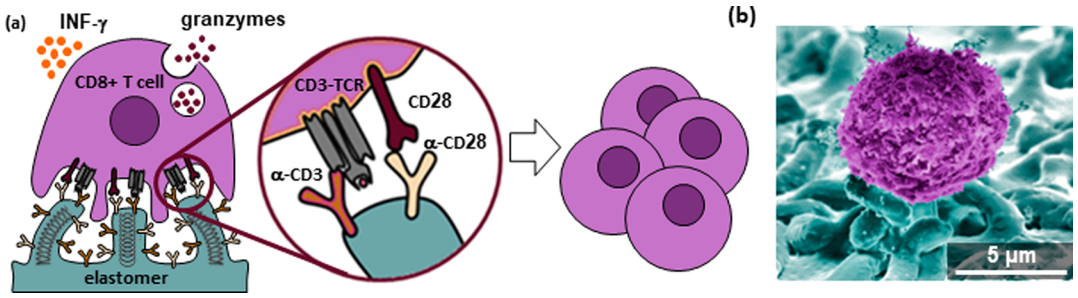

Figure 1. (a) Schematic illustration of activation and proliferation of T cells on the antibody-functionalized microbrushes. (b) Pseudo-colored SEM micrograph of a T cell stimulated on the microbrush.

TCR signaling and costimulatory CD28 signaling. However, the commercially available beads, which were initially designed for cell isolation, have never been optimized for the ex vivo activation of T cells, and they fail to reproduce physical features of the interface between T cells and their targets in vivo. One such physical feature is the mechanical stiffness of the target cell to the forces applied by T cells. It has become progressively clear that T cells are mechanosensitive and that they mechanically probe their environment to differentiate between healthy and infected cells.[9] Although the mechanosensing mechanism of T cells is still largely debated, it is obvious that a solid surface of magnetic beads can unlikely produce an optimal mechanical stimulus for T-cell activation. Several recent studies demonstrated that the elasticity of the stimulating surface largely modifies T-cell spreading[10] and alters T-cell activation and proliferation.[11,12,34]

The second key physical feature of the T cell−target interface is its microscale morphology. In vivo, T cells contact target cells using microscale actin-reach protrusions called microvilli. The topography of microvilli does not only increase the T cell−target interface but it is also believed to play a critical role in the spatial reorganization of signaling molecules that regulate the initial T-cell response. Recent studies based on super-resolution microscopy demonstrated that microvilli tips enriched with T-cell receptors (TCRs) produce tight contacts with the membrane of the target cell,[13−15] and that the shape of the microvilli promotes the spatial exclusion of large phosphatase CD45 molecules from these contacts.[16] This exclusion, in turn, shifts the kinase−phosphatase equilibrium in favor of the kinase, resulting in enhanced TCR phosphorylation and signaling.[13,17] Interestingly, topographic TCR-CD45 segregation can be artificially induced on stimulating surfaces with controlled micro-topographies at the sub-cellular scale,[18] which in turn leads to enhanced T-cell activation.[19] Furthermore, we recently stimulated T cells and NK cells on arrays of standing nanowires with tunable elasticities[20,21] and showed that both the nanowire elasticity and nanowire induced-microtopography produce distinct stimulatory effects on these cells.[22,23] Based on these fundamental studies, it can be concluded that both elasticity and micro-topography of the stimulating surface are essential regulators of T-cell response and that these regulators should be harnessed to design optimized and tunable platforms for T-cell activation and expansion.

Here, we explored a novel micro-engineered platform for ex vivo T-cell activation and proliferation that combines the stimulatory effects of surface elasticity and microtopography. The platform is based on a dense array of elastomeric micropillars functionalized with activating and costimulatory antibodies. The entire surface covered by these arrays is called hereafter "micro-brush" (Figure 1a). In general, a topography of dense standing features, such as micro-/nanoscale wires, needles, or pillars, have been broadly explored today as ex-vivo platforms for cell interactions, with the application such as gene delivery[24,25] including generation of CAR T-cell generation.[26,27] Also, elastic micropillars have been previously used for traction force microscopy aimed at studying mechanical forces exerted by cells,[28−30] as well as for the activation of helper T cells.[31] Furthermore, micropillars coated with the natural pMHC ligands for TCRs were recently used to efficiently activate cytotoxic murine T cells.[32] However, pillar-structured elastomers have never been used in combination with immunotherapeutic activating and costimulatory antibodies to enhance the activation and proliferation of human cytotoxic CD8+ T cells. In this work, we designed micropillars with various geometries and thereby altered their flexibility and compliance to the forces applied by the cells to study the effect of pillar geometry on the activation and proliferation of CD8+ T cells. We found that the micropillar topography greatly enhanced the magnitude of degranulation and cytotoxicity of T cells, when compared to those obtained from a flat surface with the same elasticity and from commercially available magnetic beads. We found, however, that T-cell activation depended on the pillar geometry, with the highest activation produced by relatively short, standing pillars that comply to the forces exerted by T cells, and allow the protrusion of the cell membrane into the areas between the pillars (Figure 1b). Surprisingly, we discovered that the micropillar-induced topography did not affect early signaling in the stimulated T cells, which suggests that the mechanism of topographically induced activation unlikely involves any modulation of TCR triggering. Finally, we found microbrush-induced activation led to the enhancement in T-cell proliferation, both in terms of proliferation magnitude and duration. These findings demonstrate that CD8+ T cells sense both the surface topography and elasticity and that an optimized microbrush is a promising alternative to the currently available platforms for therapeutic ex vivo activation and proliferation of T cells.

RESULTS

We stimulated primary human T cells on micropillars with two different lengths—5 and 10 μm, which are termed hereafter as the short and long pillars, respectively. The pillars have a diameter of 1 μm in both cases and were arranged in rectangular arrays with a periodicity of 4 μm. Since the dimension of one T cells is around 10 μm, this periodicity ensures that the one cells would contact several pillars at the same time, and always sense the topography provided by

https://doi.org/10.1021/acsami.3c01871
ACS Appl. Mater. Interfaces 2023, 15, 31103−31113

pillars. The pillars were fabricated from polydimethysiloxane (PDMS) using double replication from a silicon mold, as described in detail in the Experimental Section. The protocol used for PDMS preparation was to obtain an elastomer with an elastic modulus of ~2 MPa, which was previously shown to produce strong mechanical stimulation of T cells.[19] To provide the activating and costimulatory biochemical signals necessary to T-cell activation, the surface of pillars was functionalized with α-CD3 and α-CD28 antibodies. Notably, these surface provided two types of activating stimuli—biochemical (by ligands), and biophysical, which by itself has two components—elastic and topographical. The separate effect of the biochemical stimulus on the elastomer surface was elucidated previously,[22,33] and it is found that the antibodies were crucial for the activation. Also, to elucidate the effect of the components of the biophysical stimulus, we used three control stimulatory surfaces: (i) flat PDMS functionalized with α-CD3 and α-CD28 antibodies, which had the same elasticity as the pillars but were devoid of any stimulating microtopography, (ii) rigid glass slides functionalized with activating and costimulatory antibodies via a proadhesive poly-L-lysine (PLL) layer, and (iii) rigid glass slides functionalized with PLL only, which lacked any activating stimuli but produce good adhesion for T cells.[34] In the activation assays, commercial magnetic beads (Dynabeads) functionalized with α-CD3 and α-CD28 were used as an additional control.

At first, we studied whether the pillar topography affects the cytotoxicity of CD8+ T cells. To that end, we isolated primary human CD8+ T cells from the peripheral blood of a healthy donor, stimulated them on the pillars and the control surfaces for 3 h, and assessed the amount of exposed lysosome-associated membrane protein-1 (LAMP-1), also known as CD107a. In the activated T cells, lytic granules containing granzymes and perforins designed to induce death in target cells,[35] diffuse toward the immune synapse, where they merge with the membrane and release their lytic content into the synaptic space.[36−38] Among the structural proteins found in lytic granules is CD107a, which is brought to the surface of the membrane during the degranulation and is thus very commonly used as a quantitative marker for the activation of T cells.[38,39] Here, the amount of expressed CD107a in each T cell was assessed by immunostaining with the fluorescently labeled CD107a antibody and measuring its average fluorescence intensity per cell.

Figure 2 a and b show top-view and z-stack confocal images of T cells stimulated on short pillars for 3 h. CD107a (green) is clearly seen in a significant part of the cells stimulated on the short pillars. Figure 2c shows the average amount of degranulated CD107a signal per cell on micropillars and the control surfaces. Short PDMS micropillars showed a maximum level of activation in T cells which was significantly higher than all other surfaces. In particular, the level of CD107a expression of T cells on short PDMS micropillars was 2.5 times higher as compared to that produced by T cells incubated with the Dynabeads. Long PDMS micropillars also induced higher activation signaling as compared to Dynabeads, as well as compared to the flat PDMS functionalized with the antibodies. The lowest level of CD107a expression was obtained, as expected, for the rigid control surfaces lacking activating and costimulatory antibodies since the presence of these antibodies and the engagement of activating and costimulatory receptors they produce are critical for the T-cell activation. Interestingly, however the difference in CD107a signal between Dynabeads

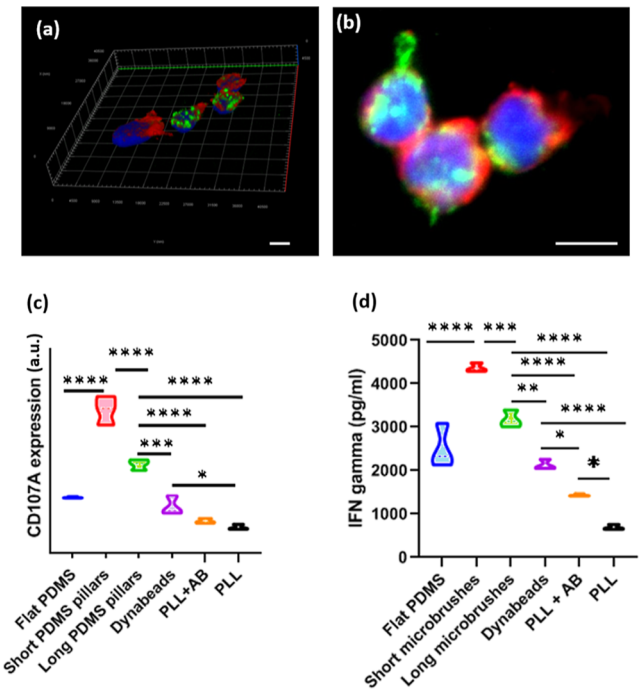

Figure 2. (a) z-stack and (b) top-view confocal images of CD8+ T cells activated on short the micropillar surfaces. The cells were stained with Alexa Fluor 555 phalloidin to visualize the cytoskeleton, DAPI for nuclei, and APC-labeled anti-CD107a as a marker of degranulation. (c) Average amount of CD107a per cell vs type of activating surface. (d) Amount of IFN-γ vs type of the activating surface. The analysis was performed with Tukey's multiple-comparison tests using GraphPad Prism software. *p < 0.05, **p < 0.01, ***p < 0.001, ****p < 0.0001, and ns: not significant. All scale bars are 5 μm.

and the rigid surface lacking the antibodies was minor and not statistically significant, the difference between Dynabeads and short micropillars was three folds in favor of the micropillars. This result suggests that the combined effect of elasticity and microtopography on the activation of T cells is at least as potent as that of the presence of activating and costimulatory molecules on an activating surface.

The positive effect of the micropillar topography on T-cell activation was confirmed by assessing the secretion of interferon-gamma (IFN-γ). IFN-γ is a cytokine with important roles in tissue homeostasis, immune and inflammatory responses, and tumor immunosurveillance. Also, IFN-γ plays cytostatic, pro-apoptotic, and antiproliferative functions in tumor immune therapies.[40−44] To quantify the secretion of IFN-γ, T cells were seeded on the micropillars and control surfaces, as well as incubated with Dynabeads for 24 h, and the supernatant was analyzed by ELISA (see the Experimental Section for details). In order to maintain the same conditions for all the cells seeded onto different surfaces, including the controls, they were mounted in chambers that exposed a constant surface area for all the cells, as well as constant volume. Figure 2d shows the IFN-γ amount vs the type of activating surface, whose trend mirrors that observed for CD107a. The highest IFN-γ level was produced by T cells activated on short micropillars. For instance, long micropillars caused a higher release of INF-γ than that on flat PDMS, Dynabeads, and rigid surfaces, yet the value was lower compared to that produced on the short micropillars. Also,

https://doi.org/10.1021/acsami.3c01871
ACS Appl. Mater. Interfaces 2023, 15, 31103−31113

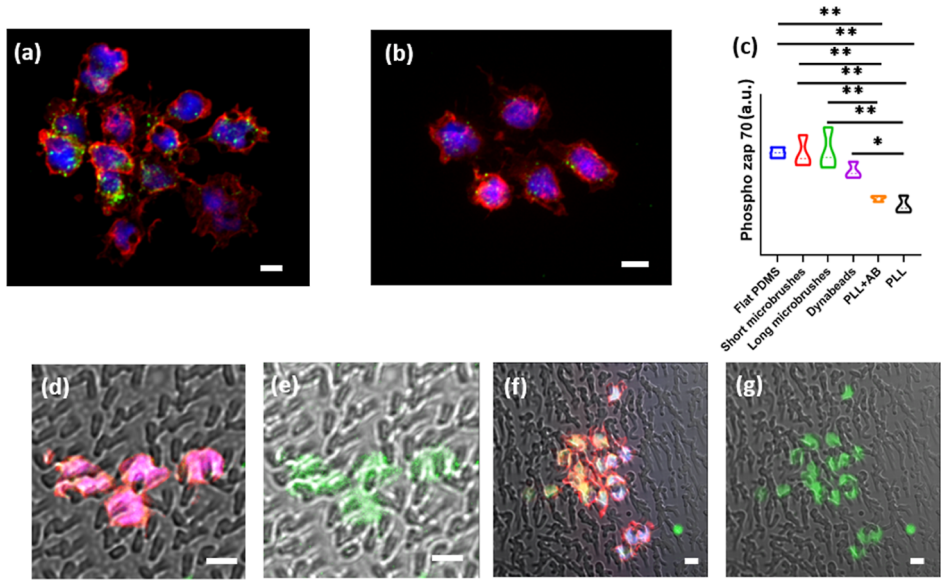

Figure 3. Confocal images of T cells showing phospho ZAP-70, after stimulation on (a) short micropillars and (b) long micropillars. Cells were stained with phalloidin for cytoskeleton (red), DAPI (blue) for nuclei, and phospho ZAP-70 (green). (c) Quantification of phospho ZAP-70 in T cells on different PDMS surfaces and controls. (d) Analysis was performed with Tukey's multiple-comparison tests using GraphPad Prism software. *$p < 0.05$, **$p < 0.01$, ***$p < 0.001$, and ****$p < 0.0001$. Combination of brightfield view of T cells stimulated on (d,e) short micropillars and on (f,g) long micropillars to view colocalization of ZAP-70. All scale bars are 5 μm.

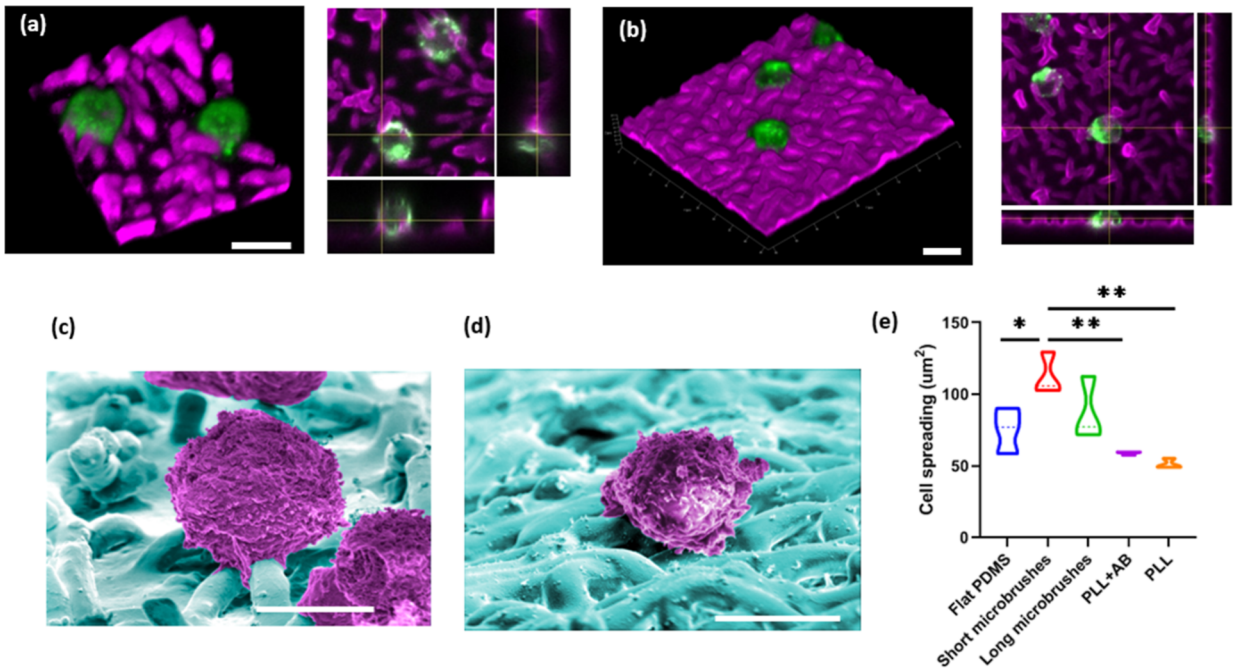

Figure 4. Mechanical interaction of human CD8+ T cells with different pillars. (a) 3D and (b) cross section *z*-stack images of T cells on the short and long micropillars. Cells were stained in green for the membrane (CellMask) and in blue for the nucleus (Dapi). To visualize the substrate topography, both surface bound mouse anti-human CD3 and CD28 were labeled with anti-mouse Alexa 647. (c,d) Pseudo-colored SEM images of T cells on the short and long micropillars, respectively. (e) Average projected cell area vs type of the stimulating surface. The analysis was performed with Tukey's multiple-comparison tests using GraphPad Prism software. *$p < 0.05$, **$p < 0.01$, ***$p < 0.001$, and ****$p < 0.0001$. All scale bars are 5 μm.

Dynabeads caused a lower INF -γ secretion than all the tested elastomeric surfaces.

To understand the mechanism underlying the enhanced activation of T cells by elastic micropillars and, specifically, to assess whether the pillar topography modifies the TCR function, we monitored TCR early signaling. In T cells, the engagement of TCR by its ligand is followed by the phosphorylation of its immune receptor activation motif (ITAM), to which the cytoplasmic tyrosine kinase ZAP-70 is recruited and phosphorylated. ZAP-70 phosphorylation, in turn, initiates downstream signal propagation and is, therefore, broadly used as a marker for the early signaling event. To assess the intensity of early TCR signaling, T cells were immobilized on the micropillars and the control surfaces for 15

https://doi.org/10.1021/acsami.3c01871
ACS Appl. Mater. Interfaces 2023, 15, 31103−31113

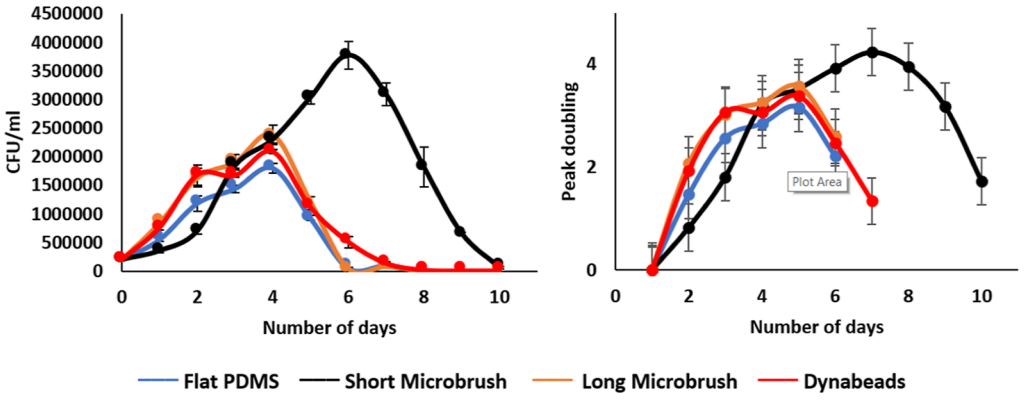

Figure 5. (a) Proliferation of human CD8+ T cells on microbrushes and control surfaces. (b) Population doubling of human CD8+ T cells on microbrushes and control surfaces.

min, fixed, and stained against ZAP-70 phosphatase by indirect immunofluorescent staining, which is a common practice to assess ZAP-70 phosphorylation.[45] The intensity of phosphorylation of ZAP-70 was quantified using confocal microscopy. Figure 3a,b show the phosphorylation of ZAP-70 in T cells on short and long micropillars, respectively, and Figure 3c shows the average signal of phospho-ZAP-70 per cell on the pillars and the control surfaces. The highest level of ZAP-70 was obtained for all PDMS-based surfaces, with no difference between them, while the lowest level was obtained for PLL-coated glass slides. Also, Dynabeads produced the early signaling that was higher than the PLL-coated surfaces yet lower than that of PDMS-based surfaces, although with no statistical significance. In addition, the intracellular location of ZAP-70 was also analyzed by immunofluorescence in T cells. The visualization with confocal microscopy (Figure 3d−g) alongside with the brightfield channel showed that ZAP-70 was not localized at the interaction point of T cells and the micropillars but was found to be dispersed all over the T cell. This can be attributed to the microstructure of the elastomeric PDMS pillars that do not enable direct access to intracellular compartments of the living cells, as seen in the case of nanowire-based platforms for T-cell activation.[46]

To better understand the nature of the mechanical interaction of T cells with the micropillars, we stained the membrane of T cells and imaged them using *z*-stack confocal microscopy. These images revealed quite different forms of short and long micropillars, their different interaction with the cell. Short micropillars, in general, maintain their standing position, and altogether produce brush-like microenvironment for T cells (hereafter termed as microbrush), which is characterized by the several distinct features. First, the cells on the microbrush (Figure 4a) seemed more spread compared to those on the long micropillars. Also, the cross-section of *z*-stack reveals that the short pillars invaginate the cell membrane, and that the cell membrane, in turn, protrudes in the interstices between the pillars. Finally, it is clearly seen that the pillars in microbrush contacted by the cells are bent toward the cell center, which suggests that these pillars complied with the centripetal forces applied by the cells. Interestingly, all these features are missing for long micropillars, which lay on the surface without producing a brush-like environment, and do not interact mechanically with the cells.

To confirm the observation of the confocal microscope, the fixed cells were dried in a critical point drier, coated with a few nanometer of Au, and imaged with a scanning electron microscope (SEM) (Figure 4 c,d). The SEM images reveal the 3D picture of the cell interaction with the surface, which is invisible in optical microscopy. First, it is clearly seen that T cells physically interact with the short pillars (Figure 4c). The pillars of the brushes produce invaginations in the cell membrane of about 1−2 μm in depth. These invaginations are used as "contact anchors" through which the cells apply forces on the pillars, as deduced from the deflection of the pillars. Furthermore, most of the pillars contacted by the cells are bent toward the cell center, suggesting that they comply with the centripetal forces applied by the cells during the early activation stage.[47] Contrary to the brushes of short micropillars, long micropillars failed to provide the anchoring contact points for T cells as they were stuck to the surface and likely formed a "carpet" of lying micropillars (Figure 4d). This was likely the reason why the shape of T cells on these surfaces was rounded and lacked invaginations. Remarkably, SEM images of the short and long pillars right after their fabrication confirmed that their tendency for standing and lying configurations, respectively, stemmed from their shapes and aspect ratios, regardless of their latter interactions with cells. Finally, the interaction of T cells with the activating surface was quantified in terms of their projected areas (Figure 4e). Here, T cells stimulated on microbrushes produced the highest area. These data largely agree with the observation from SEM and *z*-stack confocal microscopy that the topography of the short pillars, which promotes the protrusion of the cell membrane into the interstices between the micropillars, is also a trigger for the spreading of the cells.

In vivo, T-cell activation leads to T-cell proliferation, with the purpose of clonal selection and expansion of antigen-specific T cells. Also, ex vivo T-cell activation is essential for T-cell proliferation with the purpose of obtaining T-cell quantities that are sufficient for adoptive immunotherapy. To learn whether the microbrush-induced enhancement in T-cell activation can also produce the enhancement in T-cell proliferation, we carried out proliferation assays. In these assays, T cells were incubated on the short and long pillars for 24 h, re-collected, and re-cultured in a complete culture medium for 10 days, with a periodic supplement of interleukin-2 (IL-2). Antibody-functionalized flat PDMS and Dynabeads were used as control surfaces in the proliferation assays since they showed the highest activation among the control surfaces in the activation assays. The cell proliferation rate was measured each day by collecting 10 μL of the cell culture, staining it with methylene blue, and counting the cells using a

https://doi.org/10.1021/acsami.3c01871
ACS Appl. Mater. Interfaces 2023, 15, 31103−31113

flow cytometer. The culturing media was also replaced every 3 days.

Figure 5 shows the cell count vs time in days for the different activating surfaces. T cells incubated on PDMS microbrushes showed maximum proliferation as compared to Dynabeads, which are most prominently used today for T-cell proliferation. Remarkably, for Dynabeads, flat PDMS and long micropillars, T-cell numbers peaked at day 4 and rapidly declined afterward, which suggests the exhaustion of the T cells after day 4. On the contrary, the proliferation of T cells activated on the microbrushes continued to increase at a rapid rate and peaked at day 6 with a value exceeding 35×10^5 cfu/mL. After day 6, the amount of T cells activated on the microbrushes gradually decreased until day 10. T cells activated on the microbrushes showed not only a longer proliferation time but also proliferated to a substantially higher amount compared to those activated on other surfaces. Figure 5b shows the population doubling vs time. It is clearly seen that at the peak of the proliferation, the microbrush produced a population doubling index which was 30% higher than that obtained on all other surfaces at their population peak. These findings demonstrate that the microtopography of an elastic stimulating surface is an important regulator not only of the activation of T cells but also of their proliferation, yet the mechanism of this regulation still needs to be understood. Furthermore, these findings show that elastic activating surfaces with controllably structured microtopography have great potential for the controlled ex vivo activation of T cells for therapeutic surfaces.

DISCUSSION

Surfaces structures with vertical micro-/nano-topography is extensively explored nowadays for the interaction with living cells,[48] and it has been so far demonstrated for various purposes, including but not limited to the intracellular delivery of bio-materials,[49−54] traction of cellular forces,[55−58] electrical stimulation and recording intracellular electrical activity,[59] and mechanical stimulation.[30,60] Also, vertical microtopography has been used in the mechanobiological studies of lymphocyte cells[31] and the regulation of their immune function.[61] In this paper, we studied the effect of microscale topography on the activation and proliferation of T cells and demonstrated its potential in the production of T cells for immunotherapeutic purposes. In particular, we showed that microtopography could strongly increase the cytotoxicity of T cells, as revealed by both CD107a expression and INF-γ release, yet this increase is not generic but also strongly depends on topography itself. The long pillars with an aspect ratio of 10 used here did not retain their free-standing shapes but stuck to the surface. This resulted in two striking differences between short and long micropillars. The first difference is that the short micropillars produced a pronounced microbrush topography at the cell−pillar interface. This topography allowed the cells to protrude into the spaces between the pillars and restricted the cell−surface contact to the top 1−2 μm of the pillar area. On the contrary, the long micropillars, for which the pillars mostly stuck to the surface, did not produce a strong, membrane-invaginating topography and thus did not restrict the cell contact to the pillar tips. However, SEM images clearly revealed that the cells produced a relatively small contact area with the surface of the long pillars. Therefore, it can be concluded that the short, standing pillar topography acts as an artificial "enhancer" of the contact area between T cells and the stimulating surface, and this enhancement, in turn, increases the overall amount of the activating and costimulatory antibodies that trigger cell activation. This artificial enhancer can also explain why the activation using the short micropillars was significantly higher than that using Dynabeads. Importantly, to elucidate the possible effect of the antibody surface density on the activating potency of the tested surfaces, we quantified this density on each surface using fluorescent microscopy, as described in detail in the Supporting Information. We found that this surface density is within the same range for all the tested surfaces, including short and long micropillars, flat PDMS, and Dynabeads, and is above the density of antibodies required for the optimal activation of T cells on surfaces.[62] Therefore, the difference between these materials in terms of their activating efficiency of T cells cannot be attributed to the antibody density.

The second, yet no less important difference between the short and long micropillars is that the short ones greatly complied with the centripetal forces applied by T cells, as clearly seen from the z-stack and SEM images (Figure 4a−d). The result obtained here faithfully mirrors our recent reports, in which T cells and NK cells stimulated on vertical nanowires coated with activating molecules increased their activation with nanowire length, and therefore, nanowire compliance to force.[22,23] As mentioned before, there is growing evidence that such compliance to cellular forces is critical for the activation of T cells, and several studies demonstrated that decreasing the elastic modulus of the stimulating alters the activation of T cells.[12,34,75] In this sense, while all the used elastomer-based surfaces including short pillars, long pillars, and flat PDMS surfaces were made of the PDMS of the same bulk elastic modules (~2 MPa), they produced dramatically different compliances to the cell forces. Specifically, in the surface with standing pillars (microbrush), where each pillar acts as a tiny micro-spring that easily complies with the cellular forces. The bending modulus of each pillar, which is defined here as the ratio between the shear force and horizontal displacement of the pillar tip, is given by[63]

$$F/\delta = \frac{3\pi E r^4}{4l^3}$$

where F is the force, l is the pillar length, E is the Young modulus of the material, δ is the horizontal tip deflection, and r is the pillar radius. For short pillars used here, the calculated bending modulus is ~2 mPa. Thus, the microbrush with the short pillars can be viewed as an "activating continuum" structure of many highly elastic elements, and the overall effect of elasticity of this continuum is much stronger than that of a flat surface or of a nearly flat surface such as that of long micropillars.

To allow a direct comparison between how a flat surface and a surface with pillar-topography comply with the forces applied by cells, we numerically modeled this compliance using finite element analysis (Figure S3). Here, we first modeled the compliance of a pillar with a circular cross-section upon horizontal mechanical load applied on the pillar top. The dimensions and bulk elasticity of the modeled pillar were kept the same as those of the used short pillars in the cell experiments. We calculated the mechanical load (e.g., force per area of the pillar top), in Pa, required to displace the pillar top horizontally through different distances, from 1 to 5 μm. Then, we modeled the compliance of a flat surface with the same bulk

https://doi.org/10.1021/acsami.3c01871
ACS Appl. Mater. Interfaces 2023, 15, 31103−31113

elasticity (2 MPa), assuming that a horizontal force is applied to a circular area with the same diameter as the pillar top. Specifically, we applied on this area different forces with the same values obtained previously for the pillar displacement in the range of 1—5 μm and found that the displacement of the loaded area on a flat surface is 6 orders of magnitude lower than that of the pillar top, for all the forces used in the calculations. This quite intuitive observation quantitatively demonstrated how dramatic is the effect of surface microstructures and their shape on the mechanical compliance of this surface to forces exerted by cells (Figure S3).

The mechanism of elasticity-induced activation is still greatly debated and can be attributed to different features of T-cell activation. One of these is related to growing evidence that TCR is a force sensor whose change in conformation upon the applied force onto the TCR-ligand bond triggers the activation signaling.[64,65] In this context, the elasticity of the surface that supports the activating ligands greatly alters the overall load on the TCR-ligand bond, and, as a consequence, the intensity of TCR signaling. However, here the early signaling, which was characterized by the overall amount of ZAP-70 phosphatase, was the same for the short micropillars, long micropillars, and flat PDMS surface, suggesting that enhanced activation of T cells by the short micropillars is unlikely associated directly with increased TCR engagement or early signaling. While the activation time used in the ZAP-70 assays was more sufficient for the detection of early signaling,[66,75] negligible differences in ZAP-70 signals among the probed surfaces can be attributed to poor synapse was formed between the cells and the substrate. Furthermore, similar levels of ZAP-70 phosphatase produced by the brushes and PDMS surfaces suggest that the different activation levels these surfaces produced are unlikely associated with the difference in the overall contact area with T cells. We, therefore, suggest that the ability of the microbrush topography to boost T-cell activation stems rather from the ability of the standing pillars to comply with the mechanical forces at the cell−pillar interfaces. Such forces are an important regulator of T-cell activity, and they play a critical role in the formation of the immune synapse.[67] Also, the microbrush geometry allowed the stimulated cells to form protrusions, which recently were shown to be critical in the development and the upkeeping of the forces in the immune synapse and effective killing by T cells.[16] These protrusions were clearly observed in T cells on short microbrushes by SEM and confocal microscopy, and their presence correlates with the enhanced activation and cytotoxicity of T cells on these surfaces. To confirm this suggestion, we performed three control experiments, in which we stimulated T cells on short microbrushes in the presence of three protrusion inhibitors: (i) latrunculin that inhibits actin polymerization, (ii) cytochalasin that inhibits actin polymerization and induces actin depolymerization, (iii) and blebbistatin that inhibits myosin function. In all three cases, we found that the inhibitors significantly lowered the release of INF-γ compared to the non-treated cells (Figure S4).

In addition to the possible direct effect of the elasticity of the ligand-supporting substrate on TCR signaling, this elasticity also mediates T-cell activation by affecting cytoskeleton dynamics. The distal ring of the immune synapse is rich with actin, whose retrograde flow is driven by actin polymerization and myosin contraction. This flow, in turn, drives clusters of antigen receptors toward the synapse center.[68] The dynamics of this flow is an important regulator of the immune synapse,[69] and its inhibition was shown to negatively affect T-cell activation, highlighting its importance in TCR signal transduction.[70] This dynamics of actin within the immune synapse, in turn, strongly depends on the stiffness of the underlying substrate. Importantly, the cytoskeleton is linked with the T-cell environment through integrin receptors and so-called "clutch proteins".[71] The distinct feature of the clutch bond formed by the integrin is that its strength increases with the stiffness of the underlying surface. On the other hand, the increase in the mechanical coupling between the integrin complexes and cytoskeleton impedes retrograde actin flow[72] and could indirectly affect the signal propagation within the immune synapse. This linkage between the strength of TCR signal propagation and the stiffness of the T-cell environment was mirrored by several studies, in which the response of T cells activated on flat elastomeric surfaces depended on the substrate elasticity.[34,73,74]

CONCLUSIONS

The increased activation of T cells on the antibody-functionalized microbrushes led to their increased proliferation, which makes the microbrush-structured surface attractive for immunotherapeutic production of T cells. In recent years, there has been emerging research aimed at developing new nano- and microscale materials that can potentially replace magnetic beads in the process of ex vivo expansion of T cells. These materials include, but are not limited to antibody-modified nanoparticles,[75] microrods,[76] graphene,[77] polymer microfibers,[78] molecular brushes,[79] and carbon nanotubes.[80] Each of these new material approaches has its own advantages and disadvantages, but their common characteristic is that they are introduced to T cells in the soluble form. Therefore, the amount of chemical and physical stimuli received by each cell is only statistically controlled. Furthermore, these nano-/micromaterials, as well as the currently used magnetic beads, have to be completely sorted from the cells upon completion of the activation stage, which is challenging. An incomplete sorting can lead to the leftovers of the activating materials in the culture of T cells, whose effect on the therapeutic function of T cells in the patient's body is unclear. In our work, we suggest a radically different approach by which T cells are stimulated on a surface with topographical and elastic features that provide the optimal physical cues for T-cell expansion and activation. Upon activation, T cells are separated from the surface with no residues of foreign material. Furthermore, activation on the surface ensures that each T cell is exposed to nearly the same amount of physical and chemical cues, which would otherwise potentially produce high homogeneities in the resulting T-cell phenotype. Overall, our findings open a new avenue in the design of micromaterials for activation and proliferation of T cells, charting the course to more effective immunotherapies.

EXPERIMENTAL SECTION

Fabrication of PDMS Micropillars via Double Replication. Silicon master mold, containing micropillars, was created using electron beam lithography and Bosch process. The silicon master molds were first coated with trichloro(1*H*,1*H*,2*H*,2*H*-perfluorooctyl)-silane overnight under vacuum to obtain an anti-adhesive hydrophobic layer on the silicon micro pillars. Then, the Sylgard 184 PDMS kit was mixed (10:1 PDMS/hardener) and poured onto the surface of the silicon micro pillars, degassed, and then cured for an hour at 60 °C. The cured PDMS was then peeled off from the silicon and coated with anti-adhesive coating of trichloro(1*H*,1*H*,2*H*,2*H*-perfluorooctyl)-silane. This negative PDMS mold containing holes was further used

https://doi.org/10.1021/acsami.3c01871
ACS Appl. Mater. Interfaces 2023, 15, 31103−31113

for double replication by pouring PDMS (1:10) and curing at 60 °C overnight. The cured PDMS was then peeled off from the negative mold to obtain PDMS micropillars. The double replication of PDMS is a known process for fabricating PDMS micropillars[81] and was optimized to obtain micropillars of two different heights (~5 and 10 μm).

Bio-Functionalization of PDMS Micropillars. PDMS surfaces were functionalized with a mix of activating ligands α-CD3 and α-CD28. The samples were first treated in oxygen plasma for 5 s (Harrick PDC32G) and then modified with (3-aminopropyl)-triethoxysilane (APTES, Sigma-Aldrich) by immersing into a 10% ethanolic APTES solution for 10 min, rinsing with ethanol, and baking for 10 min in an oven at 60 °C.[82] The samples were incubated overnight at 4 °C in a 2 μg/mL solution of 1:1 v/v α CD3 and α CD28 in sterile phosphate-buffered saline (PBS), then rinsed three times, and stored in sterile PBS until use.

T-Cell Purification and Propagation. CD8+ T cells were isolated from fresh blood peripheral blood of a healthy adult volunteer donor, recruited by the written informed consent, as approved by the Institutional Review Board of Ben-Gurion University of the Negev. PBMCs were isolated from the blood using the FICOL gradient. First, blood is diluted in 2% FBS at a 1:1 ratio, then loaded on FICOL gradient, and centrifuged at 1200 RPM with no breaks or acceleration. The collected PBMCs were cultured in complete RPMI media with 10% human serum supplemented with 200 units of IL-2 and 50 ng OKT-3 for 2 days. Isolation of the CD8+ T cells was performed with a positive selection of CD8+ beads using a magnetic column according to the company instructions. CD8+ T cells were continuously cultured in complete RPMI media with 10% human serum supplemented with 200 units of IL-2.

Immunostaining for Phospho-Zap-70. Cultured T cells were seeded on the platforms in growth medium containing <2% serum and 50 units of IL-2 and left to adhere for 15 min. After 15 min of incubation, within which most of the early signaling occurs,[83] the cells were fixed with 4% paraformaldehyde (PFA) for 15 min at 4 °C. Then, the samples were gently rinsed with PBS, permeabilized with 0.1% Triton X100 in PBS for 3 min at 4 °C, and ice cold methanol for 10 min at −20 °C, and then blocked with 2% BSA for 1 h at 37 °C. Phospho-Zap-70 (1:50 in 2% BSA in PBS, Cell Signaling) was added on the samples and kept overnight at 4 °C. The samples were then rinsed with PBS and incubated with anti-rabbit Alexa Fluor 647 and Alexa Fluor 555 phalloidin (1:1000 and 1:40 respectively, both from Invitrogen) at room temperature for 1 h. Finally, the samples were rinsed with PBS twice, once in deionized water, and then, the nuclei were stained by mounting the samples with the ProLong Gold antifade reagent containing DAPI.

Interferon-Gamma Secretion of T Cells. IFN-γ production after stimulation of T cells on PDMS micropillars was determined by a standard sandwich immunoassay. Functionalized PDMS surfaces were incubated at 37 °C with T cells in a growth medium containing 50 units of IL-2 for 24 h, which is enough time to collect detectable levels of INFγ.[84] After the incubation period, the cells were collected and centrifuged at 1500 rpm for 5 min at 4 °C. The supernatant was then collected and analyzed for IFNγ detection. Prior to the test, 96-well plates were coated with 100 μL/well of anti-human IFNγ (capture mAb, 1 μg/well). Blocking (PBS + 10% FCS) was applied for 2 h at room temperature. Following 2 h of incubation with the supernatant, biotin anti IFNγ detection mAb (2 μg/well) was added to each well. For detection, streptavidin-HRP (Jackson, 016-030-084) diluted to 1:1000 was added for 30 min. Following copious washing, 10 μL per well of the TMB substrate (DAKO, S1599) was added to each well and left to react for 10−15 min. After the addition of a stop solution, the optical density in each well was read at 450 nm (Thermo Electron Corporation Multiskan Spectrum). Between each step, wells were washed five times with PBS containing 0.05% Tween 20 (PBST).

T-Cell Activation on Micropillars. Cultured CD8+ T cells were seeded onto PDMS surfaces in growth medium containing <2% serum and 50 units of IL-2 and left to adhere for 3 h, which is enough time to observe degranulation.[85] After 3 h of incubation, samples were rinsed twice in PBS to remove the nonadherent cells, and the adherent cells were fixed with 4% PFA and blocked with 5% BSA in PBS. The actin cytoskeleton was stained with Alexa Fluor 555 phalloidin (Invitrogen), and the nuclei were stained by mounting the samples with ProLong Gold antifade reagent containing DAPI (Both from Life Technologies). For the imaging of CD107a, a degranulation marker, the cultured T cells were seeded as mentioned before. The medium was supplemented with APC anti-human CD107a (1:1000 v/v in IL-2 poor medium, Biolegend) and was left to adhere for 3 h. The samples were rinsed twice in PBS, fixed with 4% PFA, and then directly stained with Alexa Fluor 555 phalloidin without permeabilization to prevent damage to the cell membrane. Finally, the nuclei were stained by mounting the samples with ProLong Gold antifade reagent containing DAPI.

T-Cell Proliferation. T-cell proliferation was carried out according to the standard protocol employing Dynabeads. CD8+ T cells were incubated on the activating platforms (including Dynabeads), as described previously, but this time for 24 h. The cells were then isolated from the platforms and re-cultured in complete RPMI media for 10 days to study their proliferation rates after activation. The culture was kept in a 96-well plate, 20,000 cell in 200 μL per well, according to the standard protocol of ThermoFischer for human T-cell activation and expansion with Dynabeads (https://www.thermofisher.com/il/en/home/references/protocols/proteins-expression-isolation-and-analysis/t-cell-activation-and-expansion/dynabeads-human-t-activator-cd3-cd28.html). Each day 10 μL of cells was collected and stained with methylene blue to measure the cell count using the flow cytometer. The media was replaced every third day.

Imaging the T-Cell−Micropillar Interface. Cultured CD8+ T cells were seeded onto functionalized PDMS surfaces in growth medium containing <2% serum and 50 units of IL-2 and left to adhere for 3 h 10 min before the end of incubation, the medium was supplemented with the CellMask green plasma membrane stain to a final dilution of 1:1000 (Invitrogen). After incubation, samples were rinsed twice in PBS to remove the nonadherent cells, and the adherent cells were then fixed with 4% PFA. The surface-bound mouse α-CD3 and α-CD28 antibodies were fluorescently labeled by incubation in goat anti-mouse Alexa 647 in PBS + 2% BSA overnight at 4 °C. Finally, samples were mounted with the ProLong Gold antifade reagent containing DAPI to stain the nuclei. For SEM imaging, cells were incubated on the surface, as previously described. After fixation in 4% PFA, cells were dehydrated with four successive ethanol baths, dried using critical point drying, and plated with 1−2 nm of gold to limit surface charging during imaging.

Microscopy. Confocal and *z*-stack images of cells on the various surfaces were acquired using a Zeiss LSM 880 confocal microscope and quantified using Fiji imaging software. SEM images were acquired using a FEI Verios XHR 460L scanning electron microscope and pseudo-colored using an Adobe illustrator.

Statistics. All biological experiments were performed three times. 30−60 regions were imaged and averaged for quantification. In Figures 2−5, means with SD are shown. Statistical analyses were performed by analysis of variance, and Tukey's multiple-comparison post hoc test was also performed. The results were considered to be significantly different for $P < 0.05$.

■ ASSOCIATED CONTENT

Supporting Information

The Supporting Information is available free of charge at https://pubs.acs.org/doi/10.1021/acsami.3c01871.

(PDF)

■ AUTHOR INFORMATION

Corresponding Author

Mark Schvartzman − *Department of Materials Engineering and Ilse Katz Institute for Nanoscale Science and Technology, Ben-Gurion University of the Negev, Beer-Sheva 84105,*

https://doi.org/10.1021/acsami.3c01871
ACS Appl. Mater. Interfaces 2023, 15, 31103−31113

Israel; orcid.org/0000-0002-5912-525X;
Email: marksc@bgu.ac.il

Authors

Ashish Pandey − *Department of Materials Engineering and Ilse Katz Institute for Nanoscale Science and Technology, Ben-Gurion University of the Negev, Beer-Sheva 84105, Israel*

Muhammed Iraqi − *The Shraga Segal Department of Microbiology, Immunology, and Genetics, Faculty of Health Sciences, Ben-Gurion University of the Negev, Beer-Sheva 84105, Israel*

Esti Toledo − *Department of Materials Engineering and Ilse Katz Institute for Nanoscale Science and Technology, Ben-Gurion University of the Negev, Beer-Sheva 84105, Israel*; orcid.org/0000-0003-3103-816X

Abed Al-Kader Yassin − *The Shraga Segal Department of Microbiology, Immunology, and Genetics, Faculty of Health Sciences, Ben-Gurion University of the Negev, Beer-Sheva 84105, Israel*

Eytan Podvalni − *Department of Mechanical Engineering, Ben-Gurion University of the Negev, Beer-Sheva 84105, Israel*

Shagufta Naaz − *Department of Materials Engineering and Ilse Katz Institute for Nanoscale Science and Technology, Ben-Gurion University of the Negev, Beer-Sheva 84105, Israel*

Jatin Jawhir Pandit − *Department of Materials Engineering and Ilse Katz Institute for Nanoscale Science and Technology, Ben-Gurion University of the Negev, Beer-Sheva 84105, Israel*

Carlos Ureña Martin − *Department of Materials Engineering and Ilse Katz Institute for Nanoscale Science and Technology, Ben-Gurion University of the Negev, Beer-Sheva 84105, Israel*

Guillaume Le Saux − *Department of Materials Engineering and Ilse Katz Institute for Nanoscale Science and Technology, Ben-Gurion University of the Negev, Beer-Sheva 84105, Israel*

Angel Porgador − *The Shraga Segal Department of Microbiology, Immunology, and Genetics, Faculty of Health Sciences, Ben-Gurion University of the Negev, Beer-Sheva 84105, Israel*

Complete contact information is available at: https://pubs.acs.org/10.1021/acsami.3c01871

Notes

The authors declare no competing financial interest.

■ ACKNOWLEDGMENTS

This work was funded by the Israel Science Foundation (grant # 2016//21) and the Israel Innovation Authority of the Ministry of Science, Technlogy, and Space.

■ REFERENCES

(1) June, C. H.; O'connor, R. S.; Kawalekar, O. U.; Ghassemi, S.; Milone, M. C. CAR T Cell Immunotherapy for Human Cancer. *Science* **2018**, *359*, 1361−1365.

(2) Rosenberg, S. A.; Restifo, N. P. Adoptive Cell Transfer as Personalized Immunotherapy for Human Cancer. *Science* **2015**, *348*, 62−68.

(3) Paijens, S. T.; Vledder, A.; de Bruyn, M.; Nijman, H. W. Tumor-Infiltrating Lymphocytes in the Immunotherapy Era. *Cell. Mol. Immunol.* **2020**, *18*, 842−859.

(4) Rosenberg, S. A.; Yang, J. C.; Sherry, R. M.; Kammula, U. S.; Hughes, M. S.; Phan, G. Q.; Citrin, D. E.; Restifo, N. P.; Robbins, P. F.; Wunderlich, J. R.; Morton, K. E.; Laurencot, C. M.; Steinberg, S. M.; White, D. E.; Dudley, M. E. Durable Complete Responses in Heavily Pretreated Patients with Metastatic Melanoma Using T-Cell Transfer Immunotherapy. *Clin. Cancer Res.* **2011**, *17*, 4550−4557.

(5) Stevanović, S.; Draper, L. M.; Langhan, M. M.; Campbell, T. E.; Kwong, M. L.; Wunderlich, J. R.; Dudley, M. E.; Yang, J. C.; Sherry, R. M.; Kammula, U. S.; Restifo, N. P.; Rosenberg, S. A.; Hinrichs, C. S. Complete Regression of Metastatic Cervical Cancer after Treatment with Human Papillomavirus-Targeted Tumor-Infiltrating T Cells. *J. Clin. Oncol.* **2015**, *33*, 1543−1550.

(6) Creelan, B.; Wang, C.; Teer, J.; Toloza, E.; Mullinax, J.; Yao, J.; Koomen, J.; Kim, S.; Chiappori, A.; Saller, J.; Montoya, L.; Landin, A. M.; Tanvetyanon, T.; Fang, B.; Thompson, Z.; Yu, X.; Saltos, A.; Chen, D.-T.; Conejo-Garcia, J.; Haura, E.; Antonia, S. Abstract CT056: Durable Complete Responses to Adoptive Cell Transfer Using Tumor Infiltrating Lymphocytes (TIL) in Non-Small Cell Lung Cancer (NSCLC): A Phase I Trial. *Cancer Res.* **2020**, *80*, CT056.

(7) Tran, E.; Robbins, P. F.; Lu, Y.-C.; Prickett, T. D.; Gartner, J. J.; Jia, L.; Pasetto, A.; Zheng, Z.; Ray, S.; Groh, E. M.; Kriley, I. R.; Rosenberg, S. A. T-Cell Transfer Therapy Targeting Mutant KRAS in Cancer. *N. Engl. J. Med.* **2016**, *375*, 2255−2262.

(8) Zacharakis, N.; Chinnasamy, H.; Black, M.; Xu, H.; Lu, Y.-C.; Zheng, Z.; Pasetto, A.; Langhan, M.; Shelton, T.; Prickett, T.; Gartner, J.; Jia, L.; Trebska-McGowan, K.; Somerville, R. P.; Robbins, P. F.; Rosenberg, S. A.; Goff, S. L.; Feldman, S. A. Immune Recognition of Somatic Mutations Leading to Complete Durable Regression in Metastatic Breast Cancer. *Nat. Med.* **2018**, *24*, 724−730.

(9) Basu, R.; Huse, M. Mechanical Communication at the Immunological Synapse. *Trends Cell Biol.* **2017**, *27*, 241−254.

(10) Wahl, A.; Dinet, C.; Dillard, P.; Nassereddine, A.; Puech, P. H.; Limozin, L.; Sengupta, K. Biphasic Mechanosensitivity of T Cell Receptor-Mediated Spreading of Lymphocytes. *Proc. Natl. Acad. Sci. U.S.A.* **2019**, *116*, 5908−5913.

(11) Mordechay, L.; Le Saux, G.; Edri, A.; Hadad, U.; Porgador, A.; Schvartzman, M. Mechanical Regulation of the Cytotoxic Activity of Natural Killer Cells. *ACS Biomater. Sci. Eng.* **2020**, *7*, 122−132.

(12) Saitakis, M.; Dogniaux, S.; Goudot, C.; Bufi, N.; Asnacios, S.; Maurin, M.; Randriamampita, C.; Asnacios, A.; Hivroz, C. Different TCR-induced T lymphocyte responses are potentiated by stiffness with variable sensitivity. *Elife* **2017**, *6*, No. e23190.

(13) Jung, Y.; Wen, L.; Altman, A.; Ley, K. CD45 Pre-Exclusion from the Tips of T Cell Microvilli Prior to Antigen Recognition. *Nat. Commun.* **2021**, *12*, 3872.

(14) Razvag, Y.; Neve-Oz, Y.; Sajman, J.; Yakovian, O.; Reches, M.; Sherman, E. T. T Cell Activation through Isolated Tight Contacts. *Cell Rep.* **2019**, *29*, 3506−3521.e6.

(15) Chang, V. T.; Fernandes, R. A.; Ganzinger, K. A.; Lee, S. F.; Siebold, C.; McColl, J.; Jönsson, P.; Palayret, M.; Harlos, K.; Coles, C. H.; Jones, E. Y.; Lui, Y.; Huang, E.; Gilbert, R. J. C.; Klenerman, D.; Aricescu, A. R.; Davis, S. J. Initiation of T Cell Signaling by CD45 Segregation at "Close Contacts. *Nat. Immunol.* **2016**, *17*, 574−582.

(16) Goyette, J.; Nieves, D. J.; Ma, Y.; Gaus, K. How Does T Cell Receptor Clustering Impact on Signal Transduction? *J. Cell Sci.* **2019**, *132*, jcs226423.

(17) Davis, S. J.; van der Merwe, P. A. The Kinetic-Segregation Model: TCR Triggering and Beyond. *Nat. Immunol.* **2006**, *7*, 803−809.

(18) Aramesh, M.; Mergenthal, S.; Issler, M.; Plochberger, B.; Weber, F.; Qin, X.-H.; Liska, R.; Duda, G. N.; Huppa, J. B.; Ries, J.; Schütz, G. J.; Klotzsch, E. Functionalized Bead Assay to Measure Three-Dimensional Traction Forces during T-Cell Activation. *Nano Lett.* **2020**, *21*, 507−514.

(19) Lambert, L. H.; Goebrecht, G. K. E.; De Leo, S. E.; O'Connor, R. S.; Nunez-Cruz, S.; De Li, T.; Yuan, J.; Milone, M. C.; Kam, L. C. Improving T Cell Expansion with a Soft Touch. *Nano Lett.* **2017**, *17*, 821−826.

(20) Le Saux, G.; Bar-Hanin, N.; Edri, A.; Hadad, U.; Porgador, A.; Schvartzman, M. Nanoscale Mechanosensing of Natural Killer Cells Is Revealed by Antigen-Functionalized Nanowires. *Adv. Mater.* **2019**, *31*, 1805954.

(21) Bhingardive, V.; Le Saux, G.; Edri, A.; Porgador, A.; Schvartzman, M. Nanowire Based Guidance of the Morphology and Cytotoxic Activity of Natural Killer Cells. *Small* **2021**, *17*, 2007347.

(22) Bhingardive, V.; Kossover, A.; Iraqi, M.; Khand, B.; Le Saux, G.; Porgador, A.; Schvartzman, M. Antibody-Functionalized Nanowires: A Tuner for the Activation of T Cells. *Nano Lett.* **2021**, *21*, 4241−4248.
(23) Bhingardive, V.; Edri, A.; Kossover, A.; Le Saux, G.; Khand, B.; Radinsky, O.; Iraqi, M.; Porgador, A.; Schvartzman, M. Nanowire Based Mechanostimulating Platform for Tunable Activation of Natural Killer Cells. *Adv. Funct. Mater.* **2021**, *31*, 2103063.
(24) Chen, Y.; Aslanoglou, S.; Gervinskas, G.; Abdelmaksoud, H.; Voelcker, N. H.; Elnathan, R. Cellular Deformations Induced by Conical Silicon Nanowire Arrays Facilitate Gene Delivery. *Small* **2019**, *15*, 1904819.
(25) Yoh, H. Z.; Chen, Y.; Aslanoglou, S.; Wong, S.; Trifunovic, Z.; Crawford, S.; Lestrell, E.; Priest, C.; Alba, M.; Thissen, H.; Voelcker, N. H.; Elnathan, R. Polymeric Nanoneedle Arrays Mediate Stiffness-Independent Intracellular Delivery. *Adv. Funct. Mater.* **2022**, *32*, 2104828.
(26) Chen, Y.; Mach, M.; Shokouhi, A.-R.; Yoh, H. Z.; Bishop, D. C.; Murayama, T.; Suu, K.; Morikawa, Y.; Barry, S. C.; Micklethwaite, K.; Elnathan, R.; Voelcker, N. H. Efficient Non-Viral CAR-T Cell Generation via Silicon-Nanotube-Mediated Transfection. *Mater. Today* **2023**, *63*, 8−17.
(27) Elnathan, R.; Tay, A.; Voelcker, N. H.; Chiappini, C. The Start-Ups Taking Nanoneedles into the Clinic. *Nat. Nanotechnol.* **2022**, *17*, 807−811.
(28) du Roure, O.; Saez, A.; Buguin, A.; Austin, R. H.; Chavrier, P.; Siberzan, P.; Ladoux, B. Force Mapping in Epithelial Cell Migration. *Proc. Nat. Acad. Sci. U.S.A.* **2005**, *102*, 2390−2395.
(29) Balaban, N. Q.; Schwarz, U. S.; Riveline, D.; Goichberg, P.; Tzur, G.; Sabanay, I.; Mahalu, D.; Safran, S.; Bershadsky, A.; Addadi, L.; Geiger, B. Force and Focal Adhesion Assembly: A Close Relationship Studied Using Elastic Micropatterned Substrates. *Nat. Cell Biol.* **2001**, *3*, 466−472.
(30) Fu, J.; Wang, Y. K.; Yang, M. T.; Desai, R. A.; Yu, X.; Liu, Z.; Chen, C. S. Mechanical Regulation of Cell Function with Geometrically Modulated Elastomeric Substrates. *Nat. Methods* **2010**, *7*, 733−736.
(31) Jin, W.; Tamzalit, F.; Chaudhuri, P. K.; Black, C. T.; Huse, M.; Kam, L. C. T. T cell activation and immune synapse organization respond to the microscale mechanics of structured surfaces. *Proc. Natl. Acad. Sci. U.S.A.* **2019**, *116*, 19835−19840.
(32) Basu, R.; Whitlock, B. M.; Husson, J.; Le Floc'h, A.; Jin, W.; Oyler-Yaniv, A.; Dotiwala, F.; Giannone, G.; Hivroz, C.; Biais, N.; Lieberman, J.; Kam, L. C.; Huse, M. Cytotoxic T Cells Use Mechanical Force to Potentiate Target Cell Killing. *Cell* **2016**, *165*, 100−110.
(33) O'Connor, R. S.; Hao, X.; Shen, K.; Bashour, K.; Akimova, T.; Hancock, W. W.; Kam, L. C.; Milone, M. C. Substrate Rigidity Regulates Human T Cell Activation and Proliferation. *J. Immunol.* **2012**, *189*, 1330−1339.
(34) Williamson, D. J.; Owen, D. M.; Rossy, J.; Magenau, A.; Wehrmann, M.; Gooding, J. J.; Gaus, K. Pre-Existing Clusters of the Adaptor Lat Do Not Participate in Early T Cell Signaling Events. *Nat. Immunol.* **2011**, *12*, 655−662.
(35) Aktas, E.; Kucuksezer, U. C.; Bilgic, S.; Erten, G.; Deniz, G. Relationship between CD107a Expression and Cytotoxic Activity. *Cell. Immunol.* **2009**, *254*, 149−154.
(36) Fischer, K.; Andreesen, R.; Mackensen, A. An Improved Flow Cytometric Assay for the Determination of Cytotoxic T Lymphocyte Activity. *J. Immunol. Methods* **2002**, *259*, 159−169.
(37) Chahroudi, A.; Silvestri, G.; Feinberg, M. B. Measuring T Cell-Mediated Cytotoxicity Using Fluorogenic Caspase Substrates. *Methods* **2003**, *31*, 120−126.
(38) Kannan, K.; Stewart, R. M.; Bounds, W.; Carlsson, S. R.; Fukuda, M.; Betzing, K. W.; Holcombe, R. F. Lysosome-Associated Membrane Proteins h-LAMP1 (CD107a) and h-LAMP2 (CD107b) Are Activation-Dependent Cell Surface Glycoproteins in Human Peripheral Blood Mononuclear Cells Which Mediate Cell Adhesion to Vascular Endothelium. *Cell. Immunol.* **1996**, *171*, 10−19.
(39) Betts, M. R.; Koup, R. A. Detection of T-Cell Degranulation: CD107a and B. *Methods Cell Biol.* **2004**, *75*, 497−512.
(40) Ivashkiv, L. B. IFNγ: signalling, epigenetics and roles in immunity, metabolism, disease and cancer immunotherapy. *Nat. Rev. Immunol.* **2018**, *18*, 545−558.
(41) Lilkova, E.; Petkov, P.; Ilieva, N.; Krachmarova, E.; Nacheva, G.; Litov, L. Molecular Modeling of the Effects of Glycosylation on the Structure and Dynamics of Human Interferon-Gamma. *J. Mol. Model.* **2019**, *25*, 127.
(42) Alspach, E.; Lussier, D. M.; Schreiber, R. D. Interferon γ and Its Important Roles in Promoting and Inhibiting Spontaneous and Therapeutic Cancer Immunity. *Cold Spring Harb. Perspect. Biol.* **2019**, *11*, a028480.
(43) Zaidi, M. R.; Merlino, G. The Two Faces of Interferon-γ in Cancer. *Clin. Cancer Res.* **2011**, *17*, 6118−6124.
(44) Wheelock, E. F. Interferon-Like Virus-Inhibitor Induced in Human Leukocytes by Phytohemagglutinin. *Science* **1965**, *149*, 310−311.
(45) Čemerski, S.; Das, J.; Giurisato, E.; Markiewicz, M. A.; Allen, P. M.; Chakraborty, A. K.; Shaw, A. S. The Balance between T Cell Receptor Signaling and Degradation at the Center of the Immunological Synapse Is Determined by Antigen Quality. *Immunity* **2008**, *29*, 414−422.
(46) Coffer, J. L. An Overview of Semiconducting Silicon Nanowires for Biomedical Applications. *Semicond. Silicon Nanowires Biomed. Appl.* **2022**, 1−6.
(47) Bashour, K. T.; Gondarenko, A.; Chen, H.; Shen, K.; Liu, X.; Huse, M.; Hone, J. C.; Kam, L. C. CD28 and CD3 Have Complementary Roles in T-Cell Traction Forces. *Proc. Nat. Acad. Sci. U.S.A.* **2014**, *111* (6), 2241−2246.
(48) Elnathan, R.; Barbato, M. G.; Guo, X.; Mariano, A.; Wang, Z.; Santoro, F.; Shi, P.; Voelcker, N. H.; Xie, X.; Young, J. L.; Zhao, Y.; Zhao, W.; Chiappini, C. Biointerface Design for Vertical Nanoprobes. *Nat. Rev. Mater.* **2022**, *7*, 953−973.
(49) Shalek, A. K.; Gaublomme, J. T.; Wang, L.; Yosef, N.; Chevrier, N.; Andersen, M. S.; Robinson, J. T.; Pochet, N.; Neuberg, D.; Gertner, R. S.; Amit, I.; Brown, J. R.; Hacohen, N.; Regev, A.; Wu, C. J.; Park, H. Nanowire-Mediated Delivery Enables Functional Interrogation of Primary Immune Cells: Application to the Analysis of Chronic Lymphocytic Leukemia. *Nano Lett.* **2012**, *12*, 6498−6504.
(50) Chiappini, C.; Martinez, J. O.; De Rosa, E.; Almeida, C. S.; Tasciotti, E.; Stevens, M. M. Biodegradable Nanoneedles for Localized Delivery of Nanoparticles in Vivo: Exploring the Biointerface. *ACS Nano* **2015**, *9*, 5500−5509.
(51) Carthew, J.; Abdelmaksoud, H. H.; Hodgson-Garms, M.; Aslanoglou, S.; Ghavamian, S.; Elnathan, R.; Spatz, J. P.; Brugger, J.; Thissen, H.; Voelcker, N. H.; Cadarso, V. J.; Frith, J. E. Precision Surface Microtopography Regulates Cell Fate via Changes to Actomyosin Contractility and Nuclear Architecture. *Adv. Sci.* **2021**, *8*, 2003186.
(52) Chen, Y.; Alba, M.; Tieu, T.; Tong, Z.; Minhas, R. S.; Rudd, D.; Voelcker, N. H.; Cifuentes-Rius, A.; Elnathan, R. Engineering Micro−Nanomaterials for Biomedical Translation. *Adv. NanoBiomed Res.* **2021**, *1*, 2100002.
(53) Chiappini, C.; Chen, Y.; Aslanoglou, S.; Mariano, A.; Mollo, V.; Mu, H.; De Rosa, E.; He, G.; Tasciotti, E.; Xie, X.; Santoro, F.; Zhao, W.; Voelcker, N. H.; Elnathan, R. Tutorial: Using Nanoneedles for Intracellular Delivery, **2021**, *16*, 4539−4563. DOI: 10.1038/s41596-021-00600-7
(54) Carthew, J.; Abdelmaksoud, H. H.; Cowley, K. J.; Hodgson-Garms, M.; Elnathan, R.; Spatz, J. P.; Brugger, J.; Thissen, H.; Simpson, K. J.; Voelcker, N. H.; Frith, J. E.; Cadarso, V. J. Next Generation Cell Culture Tools Featuring Micro- and Nanotopographies for Biological Screening. *Adv. Funct. Mater.* **2021**, *32*, 2100881.
(55) Tan, J. L.; Tien, J.; Pirone, D. M.; Gray, D. S.; Bhadriraju, K.; Chen, C. S. Cells Lying on a Bed of Microneedles: An Approach to Isolate Mechanical Force. *Proc. Natl. Acad. Sci. U.S.A.* **2003**, *100*, 1484−1489.

(56) Balaban, N. Q.; Schwarz, U. S.; Riveline, D.; Goichberg, P.; Tzur, G.; Sabanay, I.; Mahalu, D.; Safran, S.; Bershadsky, A.; Addadi, L.; Geiger, B. Force and focal adhesion assembly: a close relationship studied using elastic micropatterned substrates. *Nat. Cell Biol.* **2001**, *3*, 466−472.
(57) Hallstrom, W.; Lexholm, M.; Suyatin, D. B.; Hammarin, G.; Hessman, D.; Samuelson, L.; Montelius, L.; Kanje, M.; Prinz, C. N. Fifteen-Piconewton Force Detection from Neural Growth Cones Using Nanowire Arrays. *Nano Lett.* **2010**, *10*, 782−787.
(58) Lard, M.; Linke, H.; Prinz, C. N. Biosensing Using Arrays of Vertical Semiconductor Nanowires: Mechanosensing and Biomarker Detection. *Nanotechnology* **2019**, *30*, 214003.
(59) Robinson, J. T.; Jorgolli, M.; Shalek, A. K.; Yoon, M. H.; Gertner, R. S.; Park, H. Vertical Nanowire Electrode Arrays as a Scalable Platform for Intracellular Interfacing to Neuronal Circuits. *Nat. Nanotechnol.* **2012**, *7*, 180−184.
(60) Hansel, C. S.; Crowder, S. W.; Cooper, S.; Gopal, S.; João Pardelha da Cruz, M.; De Oliveira Martins, L.; Keller, D.; Rothery, S.; Becce, M.; Cass, A. E. G.; Bakal, C.; Chiappini, C.; Stevens, M. M. Nanoneedle-Mediated Stimulation of Cell Mechanotransduction Machinery. *ACS Nano* **2019**, *13*, 2913−2926.
(61) Chen, Y.; Wang, J.; Li, X.; Hu, N.; Voelcker, N. H.; Xie, X.; Elnathan, R. Emerging Roles of 1D Vertical Nanostructures in Orchestrating Immune Cell Functions. *Adv. Mater.* **2020**, *32*, 2001668.
(62) Hellmeier, J.; Platzer, R.; Eklund, A. S.; Schlichthaerle, T.; Schuetz, G. J.; Jungmann, R.; Huppa, J. B.; Sevcsik, E.; Bamieh, V.; Brameshuber, M.; Preiner, J.; Jungmann, R.; Stockinger, H.; Schütz, G. J.; Huppa, J. B.; Sevcsik, E. DNA Origami Demonstrate the Unique Stimulatory Power of Single PMHCs as T Cell Antigens. *Proc. Natl. Acad. Sci. U.S.A.* **2021**, *120*, 330a.
(63) Landau, L. D.; Lifshitz, E. M. *Theory of Elasticity*; Pergamon Press: New York, NY, 1986; Vol. 7.
(64) Gil, D.; Schamel, W. W. A.; Montoya, M.; Sánchez-Madrid, F.; Alarcón, B. Recruitment of Nck by CD3ε Reveals a Ligand-Induced Conformational Change Essential for T Cell Receptor Signaling and Synapse Formation. *Cell* **2002**, *109*, 901−912.
(65) Swamy, M.; Beck-Garcia, K.; Beck-Garcia, E.; Hartl, F. A.; Morath, A.; Yousefi, O. S.; Dopfer, E. P.; Molnár, E.; Schulze, A. K.; Blanco, R.; Borroto, A.; Martín-Blanco, N.; Alarcon, B.; Höfer, T.; Minguet, S.; Schamel, W. W. A. A Cholesterol-Based Allostery Model of T Cell Receptor Phosphorylation. *Immunity* **2016**, *44*, 1091−1101.
(66) Sachar, C.; Kam, L. C. Probing T Cell 3D Mechanosensing With Magnetically-Actuated Structures. *Front. Immunol.* **2021**, *12*, 12.
(67) Grakoui, A.; Bromley, S. K.; Sumen, C.; Davis, M. M.; Shaw, A. S.; Allen, P. M.; Dustin, M. L. The Immunological Synapse: A Molecular Machine Controlling T Cell Activation. *Science* **1999**, *285*, 221−227.
(68) Dustin, M. L.; Groves, J. T. Receptor Signaling Clusters in the Immune Synapse. *Annu. Rev. Biophys.* **2012**, *41*, 543−556.
(69) Roy, N. H.; Burkhardt, J. K. The Actin Cytoskeleton: A Mechanical Intermediate for Signal Integration at the Immunological Synapse. *Front. Cell Dev. Biol.* **2018**, *6*, 116.
(70) Campi, G.; Varma, R.; Dustin, M. L. Actin and Agonist MHC−Peptide Complex−Dependent T Cell Receptor Microclusters as Scaffolds for Signaling. *J. Exp. Med.* **2005**, *202*, 1031−1036.
(71) Case, L. B.; Waterman, C. M. Integration of Actin Dynamics and Cell Adhesion by a Three-Dimensional, Mechanosensitive Molecular Clutch. *Nat. Cell Biol.* **2015**, *17*, 955−963.
(72) Hu, K.; Ji, L.; Applegate, K. T.; Danuser, G.; Waterman-Storer, C. M. Differential Transmission of Actin Motion within Focal Adhesions. *Science* **2007**, *315*, 111−115.
(73) Saitakis, M.; Dogniaux, S.; Goudot, C.; Bufi, N.; Asnacios, S.; Maurin, M.; Randriamampita, C.; Asnacios, A.; Hivroz, C. Different TCR-Induced T Lymphocyte Responses Are Potentiated by Stiffness with Variable SensitivityDifferent TCR-Induced T Lymphocyte Responses Are Potentiated by Stiffness with Variable Sensitivity. *Elife* **2017**, *6*, No. e23190.
(74) Judokusumo, E.; Tabdanov, E.; Kumari, S.; Dustin, M. L.; Kam, L. C. Mechanosensing in T Lymphocyte Activation. *Biophys. J.* **2012**, *102*, L5−L7.
(75) Hickey, J. W.; Vicente, F. P.; Howard, G. P.; Mao, H.-Q.; Schneck, J. P. Biologically Inspired Design of Nanoparticle Artificial Antigen-Presenting Cells for Immunomodulation. *Nano Lett.* **2017**, *17*, 7045−7054.
(76) Cheung, A. S.; Zhang, D. K. Y.; Koshy, S. T.; Mooney, D. J. Scaffolds That Mimic Antigen-Presenting Cells Enable Ex Vivo Expansion of Primary T Cells. *Nat. Publ. Gr.* **2018**, *36*, 160−169.
(77) Loftus, C.; Saeed, M.; Davis, D. M.; Dunlop, I. E. Activation of Human Natural Killer Cells by Graphene Oxide-Templated Antibody Nanoclusters. *Nano Lett.* **2018**, *18*, 3282−3289.
(78) Dang, A. P.; De Leo, S.; Bogdanowicz, D. R.; Yuan, D. J.; Fernandes, S. M.; Brown, J. R.; Lu, H. H.; Kam, L. C. Enhanced Activation and Expansion of T Cells Using Mechanically Soft Elastomer Fibers. *Adv. Biosyst.* **2018**, *2*, 1700167.
(79) Hammink, R.; Weiden, J.; Voerman, D.; Popelier, C.; Eggermont, L. J.; Schluck, M.; Figdor, C. G.; Verdoes, M. Semiflexible Immunobrushes Induce Enhanced T Cell Activation and Expansion. *ACS Appl. Mater. Interfaces* **2021**, *13*, 16007−16018.
(80) Fadel, T. R.; Sharp, F. A.; Vudattu, N.; Ragheb, R.; Garyu, J.; Kim, D.; Hong, E.; Li, N.; Haller, G. L.; Pfefferle, L. D.; Justesen, S.; Herold, K. C.; Fahmy, T. M. A Carbon Nanotube−Polymer Composite for T-Cell Therapy. *Nat. Nanotechnol.* **2014**, *9*, 639−647.
(81) Pokroy, B.; Kang, S. H.; Mahadevan, L.; Aizenberg, J. Self-Organization of a Mesoscale Bristle into Ordered, Hierarchical Helical Assemblies. *Science* **2009**, *323*, 237−240.
(82) V'kovski, P.; Gerber, M.; Kelly, J.; Pfaender, S.; Ebert, N.; Braga Lagache, S.; Simillion, C.; Portmann, J.; Stalder, H.; Gaschen, V.; Bruggmann, R.; Stoffel, M. H.; Heller, M.; Dijkman, R.; Thiel, V. Determination of Host Proteins Composing the Microenvironment of Coronavirus Replicase Complexes by Proximity-Labeling. *Elife* **2019**, *8*, No. e42037.
(83) Wang, H.; Kadlecek, T. A.; Au-Yeung, B. B.; Goodfellow, H. E. S.; Hsu, L. Y.; Freedman, T. S.; Weiss, A. ZAP-70: An Essential Kinase in T-Cell Signaling. In *Cold Spring Harbor perspectives in biology*; Cold Spring Harbor Laboratory Press, 2010.
(84) Edri, A.; Shemesh, A.; Iraqi, M.; Matalon, O.; Brusilovsky, M.; Hadad, U.; Radinsky, O.; Gershoni-Yahalom, O.; Dye, J. M.; Mandelboim, O.; Barda-Saad, M.; Lobel, L.; Porgador, A. The Ebola-Glycoprotein Modulates the Function of Natural Killer Cells. *Front. Immunol.* **2018**, *9*, 1.
(85) Alter, G.; Malenfant, J. M.; Altfeld, M. CD107a as a Functional Marker for the Identification of Natural Killer Cell Activity. *J. Immunol. Methods* **2004**, *294*, 15−22.

https://doi.org/10.1021/acsami.3c01871
ACS Appl. Mater. Interfaces 2023, 15, 31103−31113